Robust State Estimation of Active Distribution Networks with Multi-source Measurements

Zhelin Liu, Peng Li, Chengshan Wang, Hao Yu, Haoran Ji, Wei Xi, and Jianzhong Wu

Abstract—The volatile and intermittent nature of distributed generators (DGs) in active distribution networks (ADNs) increases the uncertainty of operating states. The introduction of distribution phasor measurement units (D-PMUs) enhances the monitoring level. The trade-offs of computational performance and robustness of state estimation in monitoring the network states are of great significance for ADNs with D-PMUs and DGs. This paper proposes a second-order cone programming (SOCP) based robust state estimation (RSE) method considering multi-source measurements. Firstly, a linearized state estimation model related to the SOCP state variables is formulated. The phase angle measurements of D-PMUs are converted to equivalent power measurements. Then, a revised SOCP-based RSE method with the weighted least absolute value estimator is proposed to enhance the convergence and bad data identification. Multi-time slots of D-PMU measurements are utilized to improve the estimation accuracy of RSE. Finally, the effectiveness of the proposed method is illustrated in the modified IEEE 33-node and IEEE 123-node systems.

Index Terms—Active distribution network ADN, robust state estimation (RSE), second-order cone programming (SOCP), multi-source measurement, bad data identification.

NOMENCLATURE

A. Sets

$\mathcal{L}$	Set of all lines
l_i	Set of nodes connected to node i
l_i^{in}	Set of upstream nodes connected to node i
l_i^{out}	Set of downstream nodes connected to node i
$\mathcal{N}$	Set of all nodes
$\mathcal{R}$	Set of nodes with nodal current injection magnitude measurement (NCIMM)
$\wp$	Set of phases, $\wp = \{\mathrm{A}, \mathrm{B}, \mathrm{C}\}$

B. Indices

d	Index of multi-time slots of distribution phasor measurement units (D-PMUs)
i, j, f	Indices of nodes
ij	Index of lines
m	Index of supervisory control and data acquisition (SCADA) and advanced metering infrastructure (AMI) measurements
p	Index of phases
r	Index of nodes with NCIMM
s, c	Indices of nodes connected to node r
y	Index of D-PMU measurements

C. Variables

θ_i^p	Voltage phase angle in phase p at node i
$\boldsymbol{K}^1, \boldsymbol{L}^1$	Line related state variables
$\boldsymbol{K}^{\mathrm{m}}, \boldsymbol{L}^{\mathrm{m}}$	NCIMM related state variables
K_{ij}^p, L_{ij}^p	Line related state variables in phase p of line ij
K_{sc}^p, L_{sc}^p	NCIMM related state variables in phase p between nodes s and c
t	Estimation time
U_i^p	Voltage magnitude in phase p at node i
$\boldsymbol{V}$	Nodal voltage related state variable
V_i^p	Nodal voltage related state variable in phase p at node i
$\boldsymbol{x}$	Second-order cone programming (SOCP) state variables
$\boldsymbol{z}[t], \boldsymbol{w}[t], \boldsymbol{r}[t]$	Calculation measurement values, calculation weights, and residuals of multi-source measurements at estimation time t

D. Parameters

$\boldsymbol{\lambda}^1, \boldsymbol{\lambda}^{\mathrm{m}}$	Weights of SOCP state variables
b_{ij}^p	Susceptance in phase p of line ij
$b_{ij}^{p,\mathrm{sh}}$	Shunt susceptance in phase p of line ij
b_i^p	Sum of susceptance and shunt susceptance of connected lines in phase p at node i
D	Coefficient of multiple time slots of D-PMU measurements
g_{ij}^p	Conductance in phase p of line ij
g_i^p	Sum of conductance of connected lines in

	phase p at node i
M	Total number of SCADA and AMI measurements
N	Total number of nodes
N^{L}	Total number of lines
T	Sampling interval of D-PMU measurements
Y	Total number of D-PMU measurements
$Y^{\mathrm{U}}, Y^{\mathrm{I}}, Y^{\mathrm{injI}}$	Number of nodal voltage, line current, and nodal current injection magnitude measurements of D-PMUs

E. Superscript

m	Measurement values of SCADA and AMI
mP, mPI	Measurement values of D-PMUs
P, Q	Active and reactive power
U, I	Voltage and current magnitudes
UP, Uθ	Standard deviations of voltage magnitude and phase angle measurements of D-PMUs
IP, Iθ	Standard deviations of current magnitude and phase angle measurements of D-PMUs
true	True values
se	State estimation values

I. INTRODUCTION

WITH the integration of advanced measurement and communication technologies, the informatization of active distribution networks (ADNs) is constantly upgrading [1], [2]. The deployment of novel measurement equipment represented by distribution phasor measurement units (D-PMUs) [3], [4] facilitates the perception level of ADNs. Compared with the conventional measurements from supervisory control and data acquisition (SCADA) [5] and advanced metering infrastructure (AMI) [6], D-PMUs provide time-synchronized measurement data with higher sampling rates and accuracy [7]. The high-resolution D-PMU measurements make it possible to monitor and track the rapid fluctuations of distribution power flow caused by the volatile and intermittent power of distributed generators (DGs) [8], [9].

To realize the real-time monitoring and dispatching of ADNs, state estimation of distribution network is carried out to best approximate the operating states with the available measurements [10]. Owing to the higher costs, D-PMU measurements are installed in part of critical nodes of ADNs [11], which will coexist with SCADA and AMI measurements for a long time in future. State estimation considering the above-mentioned multi-source measurements has become a trend in ADNs [12], [13]. A hybrid state estimator is designed in [14] to incorporate the slow-rate SCADA as well as the fast-rate PMU measurements. Reference [15] transforms the hybrid state estimation problem into a multi-stage state estimation to mitigate the computational burden. To further cope with the computational burden and data quality challenges brought by the multi-source measurements, the indices of computation time and robustness to bad measurements of state estimation are of primary concern.

Aimed at accelerating the computational process of state estimation, the weighted least squares (WLS) estimator has been widely utilized as the objective function [10], [15]. An equality-constrained WLS method was developed in [16]. The fast decoupled state estimator [17], complex state variable based estimator [18], and distributed state estimator [19] were proposed respectively to improve the computational efficiency. Due to the non-convex and nonlinear relation between the multi-source measurements and state variables, the Gauss-Newton method is extensively employed in the iterative procedure [20]. However, due to the existence of gradient descent solution [21], the Gauss-Newton method is sensitive to the initial guess and exists convergence issues.

Although the performance of D-PMUs is improved, the issues of D-PMUs in practical networks would occur due to the sudden sensing errors, data loss, and time synchronization errors. The typical bad data ratio of PMU in practical networks is reported to range from 10% to 17% [22]. To mitigate the negative impact of bad measurements on state estimation, robust state estimation (RSE) methods such as the M-estimator [23] and exponential objective function estimator [24] are developed to enhance the robustness against bad data in multi-source measurements. The weighted least absolute value (WLAV) estimator is one of the M-estimator, and the objective function of the WLAV estimator is a linear function of measurement residuals. The interior point method was adopted to solve the WLAV problem in [25]. Reference [26] proposed a PMU-based linear programming method. Reference [27] developed an iteratively reweighted least-squares implementation to solve the WLAV state estimation. Different RSE methods were implemented in [28] and [29] to mitigate the effects of leverage points in measurements. A state estimator that remains robust against both measurements and parameter errors was proposed in [30]. Compared with the WLS method, RSE methods exhibit the advantage of rejecting bad data during the estimation process, without additional post-estimation bad data identification. However, RSE methods considering the nonlinear multi-source measurements are relatively computationally expensive.

Recently, with the need for fast and reliable global convergence of state estimation, convex programming methods present excellent performance over Gauss-Newton methods [31]. Convex relaxation approaches were proposed for solving optimal power flow problems originally [32], [33]. References [34] and [35] proposed semidefinite programming (SDP) based state estimation methods to solve the nonconvexity and guarantee convergence. In contrast to SDP methods, the second-order cone programming (SOCP) method constructs the second-order cone constraints and it is free from the complicated rank-1 constraints [36]. Thus, the SOCP method has higher computational efficiency, which has been utilized in optimal operation [37], supply restoration [38], and other scenarios of ADNs. Reference [39] proposed an RSE method for integrated electricity-heat systems.

Currently, due to the introduction of D-PMUs, the SOCP methods considering the multi-source measurements in ADNs are not fully considered. In addition, bad data fre-

quently exist in the multi-source measurements, and the bad data identification may affect the estimation accuracy and computational efficiency. It is necessary to balance the performance indices including estimation accuracy, computational efficiency, and bad data identification. Oriented to the ADNs with D-PMUs and DGs, this paper proposes an

SOCP-based RSE method considering the multi-source measurements in ADNs. The proposed method aims to combine the benefits of the robust estimation method in bad data identification and the SOCP method in estimation performance. The overall framework of the proposed method is shown in Fig. 1.
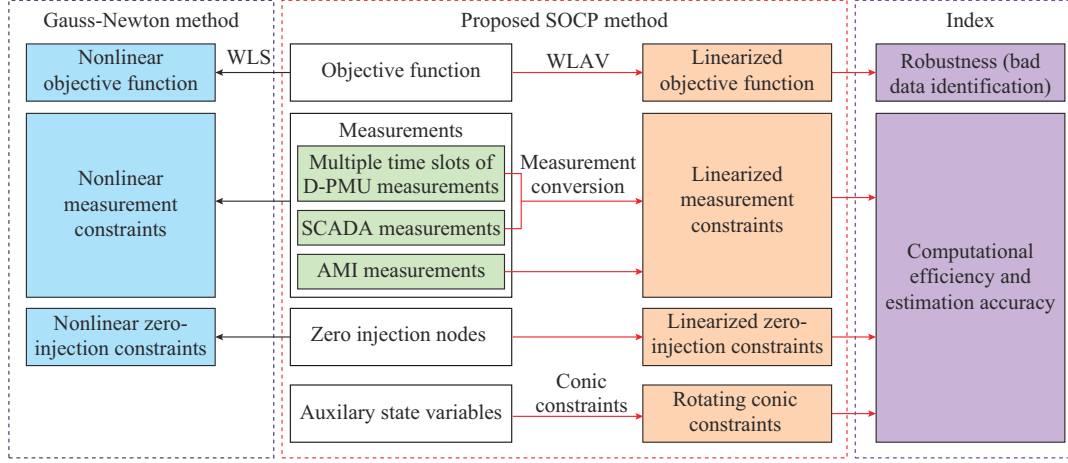

Fig. 1.   Overall framework of proposed method.

The main contributions of this paper are summarized as follows.

1) A linearized multi-source measurement model related to the SOCP state variables is formulated. Various types of multi-source measurements in ADNs are thoroughly considered, including the nodal current injection phasor measurements of D-PMUs. To enhance the applicability of the SOCP methods, the phase angle measurements of D-PMUs are converted to equivalent power measurements.

2) With the introduction of nodal current injection phasor measurements, the revised SOCP-based RSE method is proposed to enhance the robustness to bad measurement data. The WLAV estimator is selected as the objective function of RSE. The nodal current injection magnitude measurement (NCIMM) related state variables are added to the SOCP state variables. The second-order conic constraints are introduced into the RSE problem, and the effectiveness is verified by the estimation results. The robustness to the single and multiple bad measurement data of the proposed method is corroborated.

3) Considering the differences in accuracy and time scale of the multi-source measurements, the multiple time slots of D-PMU measurements are utilized to improve the estimation accuracy. The temporal correlation of D-PMU measurements is tackled in response to sudden bad measurement data.

The remainder of this paper is organized as follows. Section II builds the linearized measurement model for the SOCP-based state estimation. In Section III, the revised SOCP-based RSE method considering the multi-source measurements is elaborated. Case studies are conducted in Section IV to verify the effectiveness of the proposed method. Finally, Section V concludes this paper.

II. Linearized Measurement Model for SOCP-based State Estimation

The linearized measurement model is a prerequisite for the SOCP-based state estimation. In this section, state variables of the SOCP-based state estimation are introduced. The linearized multi-source measurement model related to the SOCP state variables is formulated.

A. State Variables of SOCP-based State Estimation

Distinct from the state variables composed of nodal voltage magnitudes and phase angles which are utilized by the Gauss-Newton method, the SOCP state variables are defined as:

$$x = [V \quad K^1 \quad L^1 \quad K^m \quad L^m]^T \tag{1}$$

where $V = (V_i^p)$; $K^1 = (K_{ij}^p)$; $L^1 = (L_{ij}^p)$; $K^m = (K_{sc}^p)$; and $L^m = (L_{sc}^p)$.

For each node i in phase p, the nodal voltage related state variable V_i^p is expressed as:

$$V_i^p = \frac{(U_i^p)^2}{\sqrt{2}} \tag{2}$$

For each line connecting nodes i and j in phase p, the line related state variables K_{ij}^p and L_{ij}^p are expressed as:

$$K_{ij}^p = U_i^p U_j^p \cos(\theta_i^p - \theta_j^p) \tag{3}$$

$$L_{ij}^p = U_i^p U_j^p \sin(\theta_i^p - \theta_j^p) \tag{4}$$

For node r with NCIMM which has more than two connecting nodes, the NCIMM related state variables K_{sc}^p and L_{sc}^p are expressed as:

$$K_{sc}^p = U_s^p U_c^p \cos(\theta_s^p - \theta_c^p) \tag{5}$$

$$L_{sc}^p = U_s^p U_c^p \sin(\theta_s^p - \theta_c^p) \tag{6}$$

B. Measurement Equations of SCADA and AMI

The considered multi-source measurements in this paper include the fast-rate D-PMU measurements and the slow-rate SCADA and AMI measurements. The differences in measurement error and time scale of the multi-source measurement equipment are reflected in the estimation weight parameter. With the introduced state variables in Section II-A, the lin-earized multi-source measurement equations are constructed. The original measurement values and standard deviations obtained from the metering instruments are partially converted to the calculation measurement values and calculation weights, respectively. To simplify the description of measurement values, residuals, calculation weights, and the standard deviations of the multi-source measurements in ADNs, Table I summarizes the multi-source measurement types and variables.

TABLE I
MULTI-SOURCE MEASUREMENT TYPES AND VARIABLES

Measurement type	Category	Measurement value at time t and $t+dT$	Residual at time t	Calculation weight at time t	Standard deviation
Nodal active and reactive power injection measurements in phase p at node i	AMI	$P_{i,p}^{\mathrm{m}}[t]$, $Q_{i,p}^{\mathrm{m}}[t]$	$r_{i,p}^{\mathrm{P}}[t]$, $r_{i,p}^{\mathrm{Q}}[t]$	$w_{i,p}^{\mathrm{P}}[t]$, $w_{i,p}^{\mathrm{Q}}[t]$	$\sigma_{i,p}^{\mathrm{P}}$, $\sigma_{i,p}^{\mathrm{Q}}$
Line sending-end/receiving-end active and reactive power measurements in phase p of line ij	SCADA	$P_{ij,p}^{\mathrm{m}}[t]$, $P_{ji,p}^{\mathrm{m}}[t]$, $Q_{ij,p}^{\mathrm{m}}[t]$, $Q_{ji,p}^{\mathrm{m}}[t]$	$r_{ij,p}^{\mathrm{P}}[t]$, $r_{ji,p}^{\mathrm{P}}[t]$, $r_{ij,p}^{\mathrm{Q}}[t]$, $r_{ji,p}^{\mathrm{Q}}[t]$	$w_{ij,p}^{\mathrm{P}}[t]$, $w_{ji,p}^{\mathrm{P}}[t]$, $w_{ij,p}^{\mathrm{Q}}[t]$, $w_{ji,p}^{\mathrm{Q}}[t]$	$\sigma_{ij,p}^{\mathrm{P}}$, $\sigma_{ji,p}^{\mathrm{P}}$, $\sigma_{ij,p}^{\mathrm{Q}}$, $\sigma_{ji,p}^{\mathrm{Q}}$
Nodal voltage magnitude measurements in phase p at node i	SCADA	$U_{i,p}^{\mathrm{m}}[t]$	$r_{i,p}^{\mathrm{U}}[t]$	$w_{i,p}^{\mathrm{U}}[t]$	$\sigma_{i,p}^{\mathrm{U}}$
	D-PMU	$U_{i,p}^{\mathrm{mP}}[t+dT]$			$\sigma_{i,p}^{\mathrm{UP}}$
Line sending-end/receiving-end current magnitude measurements in phase p of line ij	SCADA	$I_{ij,p}^{\mathrm{m}}[t]$, $I_{ji,p}^{\mathrm{m}}[t]$	$r_{ij,p}^{\mathrm{I}}[t]$, $r_{ji,p}^{\mathrm{I}}[t]$	$w_{ij,p}^{\mathrm{I}}[t]$, $w_{ji,p}^{\mathrm{I}}[t]$	$\sigma_{ij,p}^{\mathrm{I}}$, $\sigma_{ji,p}^{\mathrm{I}}$
	D-PMU	$I_{ij,p}^{\mathrm{mP}}[t+dT]$, $I_{ji,p}^{\mathrm{mP}}[t+dT]$			$\sigma_{ij,p}^{\mathrm{IP}}$, $\sigma_{ji,p}^{\mathrm{IP}}$
NCIMMs in phase p at node i	D-PMU	$I_{i,p}^{\mathrm{mP}}[t+dT]$			$\sigma_{i,p}^{\mathrm{IP}}$
Nodal voltage phase angle measurements in phase p at node i	D-PMU	$\theta_{i,p}^{\mathrm{mP}}[t+dT]$			$\sigma_{i,p}^{\mathrm{U\theta}}$
Line sending-end/receiving-end current phase angle measurements in phase p of line ij	D-PMU	$\theta_{ij,p}^{\mathrm{mP}}[t+dT]$, $\theta_{ji,p}^{\mathrm{mP}}[t+dT]$			$\sigma_{ij,p}^{\mathrm{I\theta}}$, $\sigma_{ji,p}^{\mathrm{I\theta}}$
Nodal current injection phase angle measurements in phase p at node i	D-PMU	$\theta_{i,p}^{\mathrm{mPI}}[t+dT]$			$\sigma_{i,p}^{\mathrm{I\theta}}$

1) Nodal Active and Reactive Power Injection Measurements

The nodal power injection measurements can be linearly expressed in terms of the SOCP state variables without extra transformation. The linearized measurement equations are expressed as:

$$P_{i,p}^{\mathrm{m}}[t] = -\sum_{f \in l_i^{\mathrm{in}}}\left(\sqrt{2}\, g_{fi}^p V_i^p - g_{fi}^p K_{fi}^p + b_{fi}^p L_{fi}^p\right) - \sum_{j \in l_i^{\mathrm{out}}}\left(\sqrt{2}\, g_{ij}^p V_i^p - g_{ij}^p K_{ij}^p - b_{ij}^p L_{ij}^p\right) + r_{i,p}^{\mathrm{P}}[t] \tag{7}$$

$$Q_{i,p}^{\mathrm{m}}[t] = -\sum_{f \in l_i^{\mathrm{in}}}\left[-\sqrt{2}\left(b_{fi}^p + \frac{b_{fi}^{p,\mathrm{sh}}}{2}\right)V_i^p + b_{fi}^p K_{fi}^p + g_{fi}^p L_{fi}^p\right] - \sum_{j \in l_i^{\mathrm{out}}}\left[-\sqrt{2}\left(b_{ij}^p + \frac{b_{ij}^{p,\mathrm{sh}}}{2}\right)V_i^p + b_{ij}^p K_{ij}^p - g_{ij}^p L_{ij}^p\right] + r_{i,p}^{\mathrm{Q}}[t] \tag{8}$$

The calculation weights of the nodal power injection measurements are expressed as:

$$w_{i,p}^{\mathrm{P}}[t] = \frac{1}{(\sigma_{i,p}^{\mathrm{P}})^2} \tag{9}$$

$$w_{i,p}^{\mathrm{Q}}[t] = \frac{1}{(\sigma_{i,p}^{\mathrm{Q}})^2} \tag{10}$$

2) Line Power Measurements

Since the line related state variables are expressed as the relationship between the sending-end node and the receiving-end node, the measurement equations of the sending-end and receiving-end measurements are different, which will be illustrated, respectively. The measurements of line ij are shown in Fig. 2.
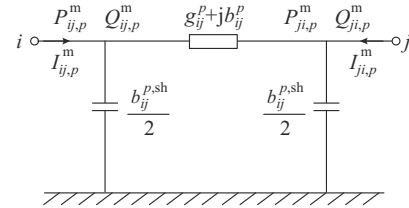

Fig. 2. Measurements of line ij.

1) Sending-end active and reactive power measurements

Similar to the nodal power injection measurements, the linearized measurement equations of the sending-end power measurements are expressed as:

$$P_{ij,p}^{\mathrm{m}}[t] = \sqrt{2}\, g_{ij}^p V_i^p - g_{ij}^p K_{ij}^p - b_{ij}^p L_{ij}^p + r_{ij,p}^{\mathrm{P}}[t] \tag{11}$$

$$Q_{ij,p}^{\mathrm{m}}[t] = -\sqrt{2}\left(b_{ij}^p + \frac{b_{ij}^{p,\mathrm{sh}}}{2}\right)V_i^p + b_{ij}^p K_{ij}^p - g_{ij}^p L_{ij}^p + r_{ij,p}^{\mathrm{Q}}[t] \tag{12}$$

The calculation weights of the sending-end power measurements are expressed as:

$$w_{ij,p}^{\mathrm{P}}[t] = \frac{1}{(\sigma_{ij,p}^{\mathrm{P}})^2} \tag{13}$$

$$w_{ij,p}^{\mathrm{Q}}[t] = \frac{1}{(\sigma_{ij,p}^{\mathrm{Q}})^2} \tag{14}$$

2) Receiving-end active and reactive power measurements

The linearized measurement equations of the receiving-end power measurements are described as:

$$P_{ji,p}^{m}[t] = \sqrt{2}\, g_{ij}^{p} V_{j}^{p} - g_{ij}^{p} K_{ij}^{p} + b_{ij}^{p} L_{ij}^{p} + r_{ji,p}^{P}[t] \tag{15}$$

$$Q_{ji,p}^{m}[t] = -\sqrt{2}\left(b_{ij}^{p} + \frac{b_{ij}^{p,\mathrm{sh}}}{2}\right)V_{j}^{p} + b_{ij}^{p} K_{ij}^{p} + g_{ij}^{p} L_{ij}^{p} + r_{ji,p}^{Q}[t] \tag{16}$$

The calculation weights of the receiving-end power measurements are expressed as:

$$w_{ji,p}^{P}[t] = \frac{1}{(\sigma_{ji,p}^{P})^{2}} \tag{17}$$

$$w_{ji,p}^{Q}[t] = \frac{1}{(\sigma_{ji,p}^{Q})^{2}} \tag{18}$$

3) Nodal Voltage Magnitude Measurements

The nodal voltage magnitude measurements are nonlinearly expressed in terms of the SOCP state variables. To construct the linearized relationship of the nodal voltage magnitude measurements, the squared voltage magnitude measurement value is chosen as the calculation measurement value, which is denoted as:

$$(U_{i,p}^{m}[t])^{2} = \sqrt{2}\, V_{i}^{p} + r_{i,p}^{U}[t] \tag{19}$$

The calculation weight of the calculation measurement value $(U_{i,p}^{m}[t])^{2}$ is related to that of the original measurement value $U_{i,p}^{m}[t]$ based on the error propagation theory [40]:

$$w_{i,p}^{U}[t] = \frac{1}{4(U_{i,p}^{m}[t]\sigma_{i,p}^{U})^{2}} \tag{20}$$

4) Line Current Magnitude Measurements

1) Sending-end current magnitude measurements

Similar to the nodal voltage magnitude measurements, the squared current magnitude measurement values are chosen as the calculation measurement values. The linearized measurement equation and calculation weight of the sending-end current magnitude measurements are expressed as:

$$(I_{ij,p}^{m}[t])^{2} = \sqrt{2}\left[(g_{ij}^{p})^{2} + \left(b_{ij}^{p} + \frac{b_{ij}^{p,\mathrm{sh}}}{2}\right)^{2}\right]V_{i}^{p} + \sqrt{2}\,((g_{ij}^{p})^{2} +$$
$$(b_{ij}^{p})^{2})V_{j}^{p} - 2\left[(g_{ij}^{p})^{2} + \left(b_{ij}^{p} + \frac{b_{ij}^{p,\mathrm{sh}}}{2}\right)b_{ij}^{p}\right]K_{ij}^{p} +$$
$$g_{ij}^{p} b_{ij}^{p,\mathrm{sh}} L_{ij}^{p} + r_{ij,p}^{I}[t] \tag{21}$$

$$w_{ij,p}^{I}[t] = \frac{1}{4(I_{ij,p}^{m}[t]\sigma_{ij,p}^{I})^{2}} \tag{22}$$

2) Receiving-end current magnitude measurements

$$(I_{ji,p}^{m}[t])^{2} = \sqrt{2}\left[(g_{ij}^{p})^{2} + \left(b_{ij}^{p} + \frac{b_{ij}^{p,\mathrm{sh}}}{2}\right)^{2}\right]V_{j}^{p} + \sqrt{2}\,((g_{ij}^{p})^{2} +$$
$$(b_{ij}^{p})^{2})V_{i}^{p} - 2\left[(g_{ij}^{p})^{2} + \left(b_{ij}^{p} + \frac{b_{ij}^{p,\mathrm{sh}}}{2}\right)b_{ij}^{p}\right]K_{ij}^{p} -$$
$$g_{ij}^{p} b_{ij}^{p,\mathrm{sh}} L_{ij}^{p} + r_{ji,p}^{I}[t] \tag{23}$$

$$w_{ji,p}^{I}[t] = \frac{1}{4(I_{ji,p}^{m}[t]\sigma_{ji,p}^{I})^{2}} \tag{24}$$

C. Measurement Equations of D-PMUs

Since the sampling rate of D-PMU measurements is significantly higher than the change in the operating state, multi-time slots of D-PMU measurements are utilized in this paper. The temporal correlation of D-PMU measurements is considered, which is aimed to improve the robustness to sudden bad measurement data in state estimation.

For each D-PMU measurement y at the estimation time t, the utilized D-PMU measurements are extended from time $t-DT$ to time $t+DT$, which is expressed as:

$$z_{y}^{P}[t] = [z_{y}^{P}[t-DT] \quad \ldots$$
$$z_{y}^{P}[t-T] \quad z_{y}^{P}[t] \quad z_{y}^{P}[t+T] \quad \ldots \quad z_{y}^{P}[t+DT]] \tag{25}$$

$$\boldsymbol{w}_{y}^{P}[t] = [w_{y}^{P}[t-DT] \quad \ldots$$
$$w_{y}^{P}[t-T] \quad w_{y}^{P}[t] \quad w_{y}^{P}[t+T] \quad \ldots \quad w_{y}^{P}[t+DT]] \tag{26}$$

$$\boldsymbol{r}_{y}^{P}[t] = [r_{y}^{P}[t-DT] \quad \ldots$$
$$r_{y}^{P}[t-T] \quad r_{y}^{P}[t] \quad r_{y}^{P}[t+T] \quad \ldots \quad r_{y}^{P}[t+DT]] \tag{27}$$

where D is an adjustable parameter to verify the validity on the improvement of estimation accuracy.

The installed D-PMU measurement types in ADNs consist of nodal voltage phasor measurements, line current phasor measurements, and nodal current injection phasor measurements. The magnitude measurements of D-PMUs can be linearly related to the SOCP state variables. However, the phase angle measurements of D-PMUs are still nonlinearly related to the SOCP state variables. To tackle the nonlinearity, the phase angle measurements of D-PMUs are converted to the corresponding line power measurements or nodal power injection measurements.

1) Nodal Voltage Magnitude Measurements of D-PMUs

Similar to the nodal voltage magnitude measurements in Section II-B, the linearized measurement equations of nodal voltage magnitude measurements of D-PMUs are extended. The variable t in (19) is replaced by $t+dT$, where $d=-D, -D+1, \ldots, D-1, D$. The linearized measurement equation and calculation weight of the nodal voltage magnitude measurements of D-PMUs are expressed as:

$$z_{y}^{P}[t+dT] = (U_{i,p}^{mP}[t+dT])^{2} = \sqrt{2}\, V_{i}^{p} + r_{y}^{P}[t+dT] \tag{28}$$

$$w_{y}^{P}[t+dT] = \frac{1}{4(U_{i,p}^{mP}[t+dT]\sigma_{i,p}^{UP})^{2}} \tag{29}$$

where the D-PMU measurement y relates to the nodal voltage magnitude measurements in phase p at node i.

2) Line Current Magnitude Measurements of D-PMUs

Similar to the line current magnitude measurements in Section II-B and the nodal voltage magnitude measurements of D-PMUs, the linearized measurement equation and calculation weight of the line current magnitude measurements of D-PMUs are no longer illustrated, which is similar to (21)-(24).

3) NCIMMs of D-PMUs

With the introduction of the NCIMMs of D-PMUs, the NCIMM related state variables are considered in this subsection. The linearized measurement equation and calculation weight of the nodal current injection magnitude measurements of D-PMUs are expressed as:

$$z_y^{\mathrm{P}}[t+dT]=(I_{i,p}^{\mathrm{mP}}[t+dT])^2=\sqrt{2}\,[(g_i^p)^2+(b_i^p)^2]V_i^p-$$
$$2\sum_{f\in l_i^{\mathrm{in}}}[(g_i^p g_{fi}^p+b_i^p b_{fi}^p)K_{fi}^p+(b_i^p g_{fi}^p-g_i^p b_{fi}^p)L_{fi}^p]-$$
$$2\sum_{j\in l_i^{\mathrm{out}}}[(g_i^p g_{ij}^p+b_i^p b_{ij}^p)K_{ij}^p-(b_i^p g_{ij}^p-g_i^p b_{ij}^p)L_{ij}^p]+$$
$$\sqrt{2}\sum_{j\in l_i}[(g_{ij}^p)^2+(b_{ij}^p)^2]V_j^p+$$
$$2\sum_{s\in l_i,c\in l_i,c>s}\sum[(g_{is}^p g_{ic}^p+b_{is}^p b_{ic}^p)K_{sc}^p-$$
$$(b_{is}^p g_{ic}^p-g_{is}^p b_{ic}^p)L_{sc}^p]+r_y^p[t+dT] \tag{30}$$

$$w_y^{\mathrm{P}}[t+dT]=\frac{1}{4(I_{i,p}^{\mathrm{mP}}[t+dT]\sigma_{i,p}^{\mathrm{IP}})^2} \tag{31}$$

where $g_i^p=\sum_{j\in l_i}g_{ij}^p$; and $b_i^p=\sum_{j\in l_i}(b_{ij}^p+b_{ij}^{p,\mathrm{sh}}/2)$.

4) Equivalent Active Power Measurements of D-PMUs

The equivalent active power measurements of D-PMUs include the sending-end active power measurements, receiving-end active power measurements, and nodal active power injection measurements. The equivalent active power measurements of D-PMUs are expressed as the correlation of related nodal voltage phasor measurements and current phasor measurements. The measurement value $P^{\mathrm{me}}[t+dT]$ and calculation weight $w_y^p[t+dT]$ of the equivalent active power measurements of D-PMUs are stated as:

$$z_y^{\mathrm{P}}[t+dT]=P^{\mathrm{me}}[t+dT]=U^{\mathrm{mP}}[t+dT]I^{\mathrm{mP}}[t+dT]\cdot$$
$$\cos(\theta^{\mathrm{mP}}[t+dT]-\theta^{\mathrm{mPI}}[t+dT]) \tag{32}$$

$$w_y^{\mathrm{P}}[t+dT]=\frac{1}{(\sigma^{\mathrm{PUM}})^2+(\sigma^{\mathrm{PIM}})^2+(\sigma^{\mathrm{PU\theta}})^2+(\sigma^{\mathrm{PI\theta}})^2} \tag{33}$$

$$\sigma^{\mathrm{PUM}}=I^{\mathrm{mP}}[t+dT]\cos(\theta^{\mathrm{mP}}[t+dT]-\theta^{\mathrm{mPI}}[t+dT])\sigma^{\mathrm{UP}} \tag{34}$$

$$\sigma^{\mathrm{PIM}}=U^{\mathrm{mP}}[t+dT]\cos(\theta^{\mathrm{mP}}[t+dT]-\theta^{\mathrm{mPI}}[t+dT])\sigma^{\mathrm{IP}} \tag{35}$$

$$\sigma^{\mathrm{PU\theta}}=-U^{\mathrm{mP}}[t+dT]I^{\mathrm{mP}}[t+dT]\sin(\theta^{\mathrm{mP}}[t+dT]-\theta^{\mathrm{mPI}}[t+dT])\sigma^{\mathrm{U\theta}} \tag{36}$$

$$\sigma^{\mathrm{PI\theta}}=U^{\mathrm{mP}}[t+dT]I^{\mathrm{mP}}[t+dT]\sin(\theta^{\mathrm{mP}}[t+dT]-\theta^{\mathrm{mPI}}[t+dT])\sigma^{\mathrm{I\theta}} \tag{37}$$

The measurement variables concerning the specific equivalent measurement types of D-PMUs are listed in Table II.

TABLE II
MEASUREMENT VARIABLES CONCERNING EQUIVALENT MEASUREMENT
TYPES OF D-PMUS

Equivalent measurement type of D-PMUs	Variable of D-PMUs					
	P^{me}	Q^{me}	U^{mP}	I^{mP}	θ^{mP}	θ^{mPI}
Equivalent sending-end active and reactive power measurements	$P_{ij,p}^{\mathrm{me}}$	$Q_{ij,p}^{\mathrm{me}}$	$U_{i,p}^{\mathrm{mP}}$	$I_{ij,p}^{\mathrm{mP}}$	$\theta_{i,p}^{\mathrm{mP}}$	$\theta_{ij,p}^{\mathrm{mP}}$
Equivalent receiving-end active and reactive power measurements	$P_{ji,p}^{\mathrm{me}}$	$Q_{ji,p}^{\mathrm{me}}$	$U_{j,p}^{\mathrm{mP}}$	$I_{ji,p}^{\mathrm{mP}}$	$\theta_{j,p}^{\mathrm{mP}}$	$\theta_{ji,p}^{\mathrm{mP}}$
Equivalent nodal active and reactive power injection measurements	$P_{i,p}^{\mathrm{me}}$	$Q_{i,p}^{\mathrm{me}}$	$U_{i,p}^{\mathrm{mP}}$	$I_{i,p}^{\mathrm{mP}}$	$\theta_{i,p}^{\mathrm{mP}}$	$\theta_{i,p}^{\mathrm{mPI}}$

The linearized measurement equations of the equivalent active power measurements of D-PMUs are similar to (7), (11), and (15), which are not illustrated here.

5) Equivalent Reactive Power Measurements of D-PMUs

Similar to the equivalent active power measurements of D-PMUs, the measurement value $Q^{\mathrm{me}}[t+dT]$ and calculation weight $w_y^{\mathrm{P}}[t+dT]$ of the equivalent reactive power measurements of D-PMUs are expressed as:

$$z_y^{\mathrm{P}}[t+dT]=Q^{\mathrm{me}}[t+dT]=U^{\mathrm{mP}}[t+dT]I^{\mathrm{mP}}[t+dT]\cdot$$
$$\sin(\theta^{\mathrm{mP}}[t+dT]-\theta^{\mathrm{mPI}}[t+dT]) \tag{38}$$

$$w_y^{\mathrm{P}}[t+dT]=\frac{1}{(\sigma^{\mathrm{QUM}})^2+(\sigma^{\mathrm{QIM}})^2+(\sigma^{\mathrm{QU\theta}})^2+(\sigma^{\mathrm{QI\theta}})^2} \tag{39}$$

$$\sigma^{\mathrm{QUM}}=I^{\mathrm{mP}}[t+dT]\sin(\theta^{\mathrm{mP}}[t+dT]-\theta^{\mathrm{mPI}}[t+dT])\sigma^{\mathrm{UP}} \tag{40}$$

$$\sigma^{\mathrm{QIM}}=U^{\mathrm{mP}}[t+dT]\sin(\theta^{\mathrm{mP}}[t+dT]-\theta^{\mathrm{mPI}}[t+dT])\sigma^{\mathrm{IP}} \tag{41}$$

$$\sigma^{\mathrm{QU\theta}}=U^{\mathrm{mP}}[t+dT]I^{\mathrm{mP}}[t+dT]\cos(\theta^{\mathrm{mP}}[t+dT]-\theta^{\mathrm{mPI}}[t+dT])\sigma^{\mathrm{U\theta}} \tag{42}$$

$$\sigma^{\mathrm{QI\theta}}=-U^{\mathrm{mP}}[t+dT]I^{\mathrm{mP}}[t+dT]\cos(\theta^{\mathrm{mP}}[t+dT]-\theta^{\mathrm{mPI}}[t+dT])\sigma^{\mathrm{I\theta}} \tag{43}$$

The linearized measurement equations of the equivalent reactive power measurements of D-PMUs are similar to (8), (12), and (16), which are not illustrated here.

D. Measurement Equations of Zero Injection Nodes

For any zero injection node i without any loads and DGs, the zero injection constraints at node i in phase p are constructed as:

$$-\sum_{f\in l_i^{\mathrm{in}}}(\sqrt{2}\,g_{fi}^p V_i^p-g_{fi}^p K_{fi}^p+b_{fi}^p L_{fi}^p)-$$
$$\sum_{j\in l_i^{\mathrm{out}}}(\sqrt{2}\,g_{ij}^p V_i^p-g_{ij}^p K_{ij}^p-b_{ij}^p L_{ij}^p)=0 \tag{44}$$

$$-\sum_{f\in l_i^{\mathrm{in}}}\left[-\sqrt{2}\left(b_{fi}^p+\frac{b_{fi}^{p,\mathrm{sh}}}{2}\right)V_i^p+b_{fi}^p K_{fi}^p+g_{fi}^p L_{fi}^p\right]-$$
$$\sum_{j\in l_i^{\mathrm{out}}}\left[-\sqrt{2}\left(b_{ij}^p+\frac{b_{ij}^{p,\mathrm{sh}}}{2}\right)V_i^p+b_{ij}^p K_{ij}^p-g_{ij}^p L_{ij}^p\right]=0 \tag{45}$$

III. REVISED SOCP-BASED RSE METHOD

To combine the benefits of the WLAV estimation method in bad data identification and the SOCP method in estimation performance, a revised SOCP-based RSE method is proposed in this section.

A. Modeling of WLAV-based SOCP Method

The WLAV-based state estimation model considering the multi-source measurements in ADNs is formulated as:

$$\begin{cases}\min_{x}\ J(x)=\boldsymbol{w}^{\mathrm{T}}[t]\,|\,\boldsymbol{r}[t]\,| \\ \text{s.t.}\ \ z[t]=\boldsymbol{H}\boldsymbol{x}+\boldsymbol{r}[t] \\ \quad\ \ \boldsymbol{C}\boldsymbol{x}=0\end{cases} \tag{46}$$

$$z[t]=[z_1^{\mathrm{SA}}[t]\ \ z_2^{\mathrm{SA}}[t]\ \ \cdots$$
$$z_m^{\mathrm{SA}}[t]\ \ \cdots\ \ z_M^{\mathrm{SA}}[t]\ \ z_1^{\mathrm{P}}[t]\ \ z_2^{\mathrm{P}}[t]\ \ \cdots\ \ z_y^{\mathrm{P}}[t]\ \ \cdots\ \ z_Y^{\mathrm{P}}[t]]^{\mathrm{T}} \tag{47}$$

$$\boldsymbol{w}[t]=[w_1^{\mathrm{SA}}[t]\ \ w_2^{\mathrm{SA}}[t]\ \ \cdots\ \ w_m^{\mathrm{SA}}[t]\ \ \cdots$$
$$w_M^{\mathrm{SA}}[t]\ \ \boldsymbol{w}_1^{\mathrm{P}}[t]\ \ \boldsymbol{w}_2^{\mathrm{P}}[t]\ \ \cdots\ \ \boldsymbol{w}_y^{\mathrm{P}}[t]\ \ \cdots\ \ \boldsymbol{w}_Y^{\mathrm{P}}[t]]^{\mathrm{T}} \tag{48}$$

$$r[t]=[r_1^{\mathrm{SA}}[t] \quad r_2^{\mathrm{SA}}[t] \quad \ldots \quad r_m^{\mathrm{SA}}[t] \quad \ldots$$
$$r_M^{\mathrm{SA}}[t] \ r_1^{\mathrm{P}}[t] \ r_2^{\mathrm{P}}[t] \ \ldots \ r_y^{\mathrm{P}}[t] \ \ldots \ r_Y^{\mathrm{P}}[t]]^{\mathrm{T}} \tag{49}$$

where $z[t]$ is constituted by (7), (8), (11), (12), (15), (16), (19), (21), (23), (28), (30), (32), and (38); $w[t]$ is constituted by (9), (10), (13), (14), (17), (18), (20), (22), (24), (29), (31), (33), and (39); H is the compact matrix form of linearized measurement equations constituted by (7), (8), (11), (12), (15), (16), (19), (21), and (23); and C is the compact matrix form of (44) and (45).

To alleviate the nonconvexity caused by the absolute value variable $|r|$, the auxiliary variables u and v are introduced as:

$$\begin{cases} u = \dfrac{|r|-r}{2} \\[2mm] v = \dfrac{|r|+r}{2} \end{cases} \tag{50}$$

The equivalent model of (46) is transformed into:

$$\begin{cases} \min\limits_{x} \ J(x) = w^{\mathrm{T}}[t](u+v) \\ \text{s.t.} \ z[t] = Hx + v - u \\ \quad Cx = 0 \\ \quad u \geq 0 \\ \quad v \geq 0 \end{cases} \tag{51}$$

Since the number of the SOCP state variables is larger than that of state variables in the traditional Gauss-Newton method $2N$ considering D-PMUs, it may lead to the unobservability of RSE. To solve the unobservability problem, the second-order cone constraints are introduced into the WLAV problem.

The equality constraints (52) and (53) are satisfied between the SOCP state variables.

$$(K_{ij}^p)^2 + (L_{ij}^p)^2 = 2V_i^p V_j^p \quad \forall ij \in \mathcal{L}, \forall p \in \wp \tag{52}$$

$$(K_{sc}^p)^2 + (L_{sc}^p)^2 = 2V_s^p V_c^p \quad s \in l_r, c \in l_r, c > s, \forall r \in \mathcal{R}, \forall p \in \wp \tag{53}$$

The above equality constraints are relaxed into the rotating second-order cone constraints:

$$(K_{ij}^p)^2 + (L_{ij}^p)^2 \leq 2V_i^p V_j^p \quad \forall ij \in \mathcal{L}, \forall p \in \wp \tag{54}$$

$$(K_{sc}^p)^2 + (L_{sc}^p)^2 \leq 2V_s^p V_c^p \quad s \in l_r, c \in l_r, c > s, \forall r \in \mathcal{R}, \forall p \in \wp \tag{55}$$

To make the second-order cone constraints close to the equality constraints (52) and (53), the term $-(\lambda^1(K^1)^{\mathrm{T}} + \lambda^{\mathrm{m}}(K^{\mathrm{m}})^{\mathrm{T}})$ is added to the objective function. Then, the model of the SOCP-based RSE method is transformed into:

$$\begin{cases} \min\limits_{x} \ J(x) = -(\lambda^1(K^1)^{\mathrm{T}} + \lambda^{\mathrm{m}}(K^{\mathrm{m}})^{\mathrm{T}}) + w^{\mathrm{T}}[t](u+v) \\ \text{s.t.} \ z[t] = Hx + v - u \\ \quad Cx = 0 \\ \quad (K_{ij}^p)^2 + (L_{ij}^p)^2 \leq 2V_i^p V_j^p \quad \forall ij \in \mathcal{L}, \forall p \in \wp \\ \quad (K_{sc}^p)^2 + (L_{sc}^p)^2 \leq 2V_s^p V_c^p \quad s \in l_r, c \in l_r, c > s, \forall r \in \mathcal{R}, \forall p \in \wp \\ \quad u \geq 0 \\ \quad v \geq 0 \end{cases} \tag{56}$$

B. Observability of SOCP-based RSE Method

The number of the multi-source measurements in the Gauss-Newton method is $M^{\mathrm{GN}} = M + Y = M + 2(Y^{\mathrm{U}} + Y^{\mathrm{I}} + Y^{\mathrm{injI}})$. With the introduced equivalent power measurements, the number of the multi-source measurements in the SOCP method is $M^{\mathrm{SOCP}} = M + Y^{\mathrm{U}} + 3Y^{\mathrm{I}} + 3Y^{\mathrm{injI}}$. Compared with the Gauss-Newton method, the number M^{SOCP} is increased by $Y^{\mathrm{I}} + Y^{\mathrm{injI}} - Y^{\mathrm{U}}$. In addition, the second-order cone constraints make the equivalent measurements increase by $N^{\mathrm{L}} + Y^{\mathrm{injI}}$. Compared with the Gauss-Newton method, the variation of the number of the multi-source measurements is $Y^{\mathrm{I}} + 2Y^{\mathrm{injI}} - Y^{\mathrm{U}} + N^{\mathrm{L}}$. For radial distribution networks, $N^{\mathrm{L}} = N - 1$; thus, the variation of the number of the multi-source measurements between the Gauss-Newton method and the SOCP method is $Y^{\mathrm{I}} + 2Y^{\mathrm{injI}} - Y^{\mathrm{U}} + N - 1$.

The number of state variables in the Gauss-Newton method n^{GN} is $2N$ considering D-PMUs. However, with the introduction of auxiliary state variables, the number of state variables in the SOCP method n^{SOCP} reaches $N + 2N^{\mathrm{L}} + 2Y^{\mathrm{injI}} = 3N + 2Y^{\mathrm{injI}} - 2$. Compared with the Gauss-Newton method, the number of state variables is increased by $N + 2Y^{\mathrm{injI}} - 2$.

Since Y^{I} is larger than Y^{U}, the variation of the number of the multi-source measurements $Y^{\mathrm{I}} + 2Y^{\mathrm{injI}} - Y^{\mathrm{U}} + N - 1$ is larger than the variation of the number of state variables $N + 2Y^{\mathrm{injI}} - 2$. It indicates that the introduction of measurement conversion and second-order cone constraints ensures the observability of the SOCP-based RSE.

C. Solution of SOCP-based RSE Method

To solve the above SOCP-based RSE problem, the interior-point algorithm is utilized where the dual problem of the primal problem (56) is formulated [41]. The interior-point algorithm solver deals with the primal optimal solution and the dual optimal solution simultaneously. Then, the optimal primal-dual solution will be obtained by given termination tolerance, which is usually selected as the gap of the objective function between the primal problem and the dual problem.

In this paper, the RSE problem (56) is solved by the optimization software MOSEK [42]. The estimation values of the SOCP state variables x are obtained, and the estimation results are recovered to the original voltage magnitudes and phase angles.

1) Estimation Values of Nodal Voltage Magnitudes

For any node i, the estimation value of nodal voltage magnitude U_i^p can be obtained from the SOCP state variable V_i^p as:

$$U_i^p = \sqrt{\sqrt{2}\,V_i^p} \tag{57}$$

2) Estimation Values of Nodal Voltage Phase Angles

The estimation values of nodal voltage phase angles at the source node in phases A, B, and C are set equal to 0, $-2\pi/3$, and $2\pi/3$, respectively. For any line connecting nodes i and j, the estimation values of nodal voltage phase angles satisfy the following relationship:

$$\theta_j^p = \theta_i^p - \arctan\frac{L_{ij}^p}{K_{ij}^p} \tag{58}$$

Starting from the source node, the voltage phase angles of

all other nodes can be obtained by using the breadth-first search algorithm or the depth-first search algorithm.

D. Implementation of SOCP-based RSE Method

Figure 3 depicts the flowchart of the proposed SOCP-based RSE method.
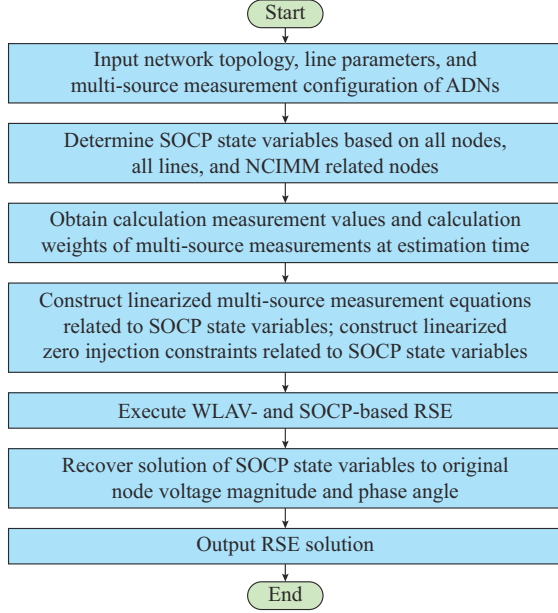

Fig. 3.   Flowchart of proposed SOCP-based RSE method.

Due to the mutual decoupling between phases of the second-order cone constraints (54) and (55), the proposed RSE method is applicable to multi-phase balanced networks and multi-phase decoupled unbalanced networks, and the unbalance of loads can be treated.

IV. CASE STUDIES AND ANALYSIS

In this section, the effectiveness of the proposed SOCP-based RSE method considering multi-source measurements is verified in the modified IEEE 33-node and 123-node systems. The proposed method is programmed using C++ and solved by MOSEK. The numerical experiments are carried out on a computer with an Intel Xeon CPU E5-2650 v2 processor running at 2.60 GHz and 20 GB of RAM.

A. Modified IEEE 33-node System

The topology and multi-source measurement configuration of the modified IEEE 33-node system is presented in Fig. 4, of which the rated voltage level is 12.66 kV. Nodes 2, 3, and 6 are modified as zero injection nodes, which represent the switching stations in practical networks.

To simulate the multi-source measurement data, their true values are obtained by the distribution power flow analysis. Then, the Gaussian distributed measurement noises are added to the true values. The standard deviations of the multi-source measurements are listed in Table III.

For the magnitude measurements of D-PMUs, SCADA, and AMI, the measurement value satisfies:

● Nodal voltage magnitude (SCADA); — Line current magnitude (SCADA);
— Line power (SCADA); ● Nodal voltage phasor (D-PWU)
— Line current phasor (D-PWU); → Nodal current injection phasor (D-PWU);
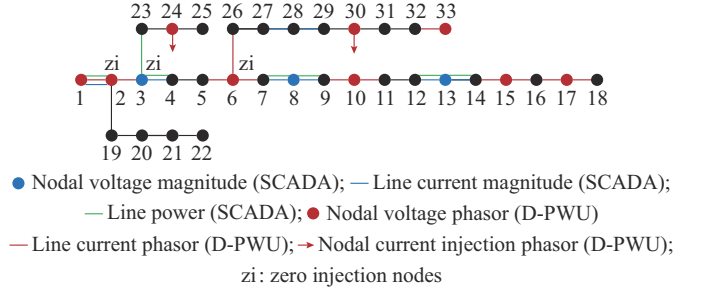zi: zero injection nodes

Fig. 4.   Topology and multi-source measurement configuration of modified IEEE 33-node system.

TABLE III
STANDARD DEVIATIONS OF MULTI-SOURCE MEASUREMENTS

Measurement type	Standard deviation of measurement errors
Magnitude measurements of D-PMUs	0.1%
Phase angle measurements of D-PMUs	0.01°
Measurements of SCADA	1%
Measurements of AMI	5%

$$z^{\mathrm{mea}} = z^{\mathrm{true}}(1+e) \tag{59}$$

where z^{mea} and z^{true} are the measurement value and true value, respectively; and e is the added measurement noise.

For the phase angle measurements of D-PMUs, the measurement value satisfies:

$$z^{\mathrm{mea}} = z^{\mathrm{true}} + e \tag{60}$$

B. Estimation Accuracy and Convergence Analysis

To assess the estimation accuracy, convergence, and computation time of the proposed method, 250 Monte Carlo simulations are performed, and the total time of state estimation T^{tot} is listed. The following four indices are utilized to assess the estimation accuracy.

1) Average relative errors of nodal voltage magnitudes U^{re}

$$U^{\mathrm{re}} = \frac{1}{N}\sum_{i\in\mathcal{N}}\left|\frac{U_i^{\mathrm{se}} - U_i^{\mathrm{true}}}{U_i^{\mathrm{true}}}\right| \tag{61}$$

2) Average absolute errors of nodal voltage phase angles θ^{ae}

$$\theta^{\mathrm{ae}} = \frac{1}{N}\sum_{i\in\mathcal{N}}\left|\theta_i^{\mathrm{se}} - \theta_i^{\mathrm{true}}\right| \tag{62}$$

3) Average relative errors of nodal power injections E^{re}

$$E^{\mathrm{re}} = \frac{1}{2N}\sum_{i\in\mathcal{N}}\left(\left|\frac{P_i^{\mathrm{se}} - P_i^{\mathrm{true}}}{P_i^{\mathrm{true}}}\right| + \left|\frac{Q_i^{\mathrm{se}} - Q_i^{\mathrm{true}}}{Q_i^{\mathrm{true}}}\right|\right) \tag{63}$$

4) Average absolute errors of nodal power injections E^{ae}

$$E^{\mathrm{ae}} = \frac{1}{2N}\sum_{i\in\mathcal{N}}\left(\left|P_i^{\mathrm{se}} - P_i^{\mathrm{true}}\right| + \left|Q_i^{\mathrm{se}} - Q_i^{\mathrm{true}}\right|\right) \tag{64}$$

The solution of the proposed SOCP-based RSE method (WLAV-SOCP) is compared with the WLS-based Gauss-Newton (WLS-GN) method and the WLAV-based Gauss-

Newton (WLAV-GN) method in [27]. The weights of the SOCP state variables λ^l and λ^m are set to be 10^{-4} and 10^{-2}, respectively. The termination tolerance of the WLS-GN and WLAV-GN methods is set to be 10^{-5} per unit, while that of the WLAV-SOCP method is set to be 10^{-8} per unit. The maximum iteration number is set to be 100 to ensure the convergence of state estimation. Simulation scenarios with different multi-source measurement configurations are implemented to verify the estimation performance of the proposed method.

1) Multi-source Measurements Without D-PMUs

To evaluate the second-order cone relaxations on the estimation performance, the D-PMU measurements in Fig. 4 are not considered, that is, only the conventional SCADA and AMI measurements are taken into consideration. Except the source node 1 and the zero injection nodes, all other nodes are equipped with AMI measurements.

The results in Table IV show the estimation accuracy and total computation time of the three methods. With the introduced second-order cone relaxations, the estimation errors of the WLAV-SOCP method are slighter than those of the WLS-GN method and the WLAV-GN method, but are still at the same error level. The total computation time of the WLAV-SOCP method is between that of the WLS-GN method and the WLAV-GN method. Because of the linear objective function in the WLAV-GN method, its computation time is the longest. The iteration number to achieve convergence of the WLAV-GN method is analyzed in Table V, where different maximum iteration numbers are assigned, respectively.

TABLE IV
COMPARISON OF STATE ESTIMATION RESULTS WITHOUT D-PMUS

Method	U^{re} (%)	θ^{ae} (°)	E^{re} (%)	E^{ae} (kW)	T^{tot} (s)
WLS-GN	0.5767	0.0141	6.5740	1.5878	6.106
WLAV-GN	0.4804	0.0143	6.4795	1.4744	15.280
WLAV-SOCP	0.7018	0.0165	7.0577	1.8151	11.337

Note: total computation time T^{tot} refers to total time of 250 simulations.

TABLE V
CONVERGENCE OF WLAV-GN METHOD

The maximum iteration number	Non-converge state estimation number
25	75
50	11
100	0

The results show that when the maximum iteration number is 50, 11 times of the WLAV-GN estimation are not convergent with the termination tolerance of 10^{-5}. All the state estimations are convergent with the maximum iteration number 100. In contrast, the proposed WLAV-SOCP method achieves the estimation convergence rate of 100%.

2) Multi-source Measurements Considering D-PMUs

The multi-source measurements considering the D-PMU measurements in Fig. 4 are analyzed, in which the impact of measurement conversion of D-PMUs is tested. To verify the effectiveness of the NCIMM related state variables, the nod-

al current injection phasor measurements are distributed at nodes 24 and 30. Except for nodes 1, 2, 3, 6, 24, and 30, all other nodes are equipped with AMI measurements. The measurement redundancy is 1.909. The estimation results of different state estimation methods considering D-PMUs are shown in Table VI.

TABLE VI
COMPARISON OF ESTIMATION RESULTS OF DIFFERENT STATE ESTIMATION METHODS CONSIDERING D-PMUS

Method	U^{re} (%)	θ^{ae} (°)	E^{re} (%)	E^{ae} (kW)	T^{tot} (s)
WLS-GN	0.1138	0.0241	4.7592	0.9786	7.255
WLAV-GN	0.0356	0.0044	4.9222	0.9918	10.289
WLAV-SOCP	0.0482	0.0032	4.3695	1.0682	13.155

The estimation results in Table VI reveal that compared with the utilization of original D-PMU measurement values in the WLS-GN and WLAV-GN methods, the measurement conversion in the WLAV-SOCP method facilitates the implementation of the SOCP methods. The estimation accuracy in the nodal voltage phase angles of the WLAV-SOCP method is improved. The total computation time of the proposed WLAV-SOCP method with D-PMU measurements is close to the WLAV-GN method.

Different coefficients of multi-time slots of D-PMUs, i.e., D, are considered to improve the estimation accuracy of the WLAV-SOCP method. The results in Table VII and Fig. 5 show that as the coefficient D increases to 1, the estimation errors of nodal voltage magnitudes reduce to 0.0250%, which outperform the other two methods. Meanwhile, the computation time of the WLAV-SOCP method increases with the coefficient D. The results in Table VII further indicate that due to the relatively small number of D-PMUs, the impact of multi-time slots of D-PMU measurements on the estimation errors of nodal power injections is not obvious. Thus, we consider configuring more D-PMUs in the network.

TABLE VII
WLAV-SOCP BASED STATE ESTIMATION RESULTS WITH DIFFERENT COEFFICIENTS OF MULTI-TIME SLOTS OF D-PMUS

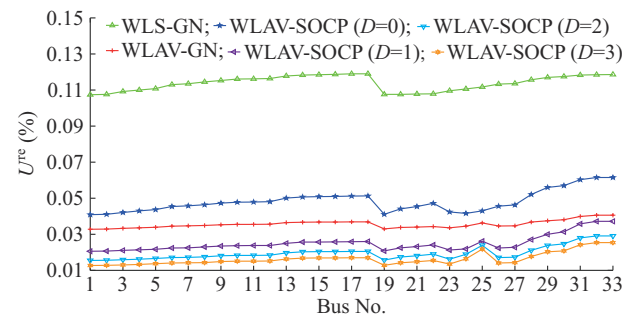| D	U^{re} (%)	θ^{ae} (°)	E^{re} (%)	E^{ae} (kW)	T^{tot} (s)
0	0.0482	0.0032	4.3695	1.0682	13.155
1	0.0250	0.0030	4.1702	1.0260	23.223
2	0.0196	0.0030	4.1419	1.0130	27.157
3	0.0164	0.0029	4.0774	1.0098	33.121

Fig. 5. Estimation errors of nodal voltage magnitudes.

3) More D-PMUs in Multi-source Measurements

Based on the multi-source measurement configurations in Fig. 4, more D-PMU and SCADA measurements are configured, as shown in Fig. 6. The measurement redundancy is 2.485. The estimation results of different state estimation methods are shown in Table VIII and Fig. 7.
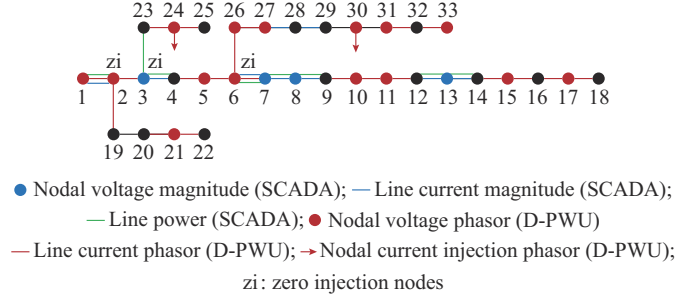

Fig. 6. Structure of modified IEEE 33-node system with more D-PMU and SCADA measurements.

TABLE VIII
COMPARISON OF STATE ESTIMATION RESULTS WITH DIFFERENT METHODS

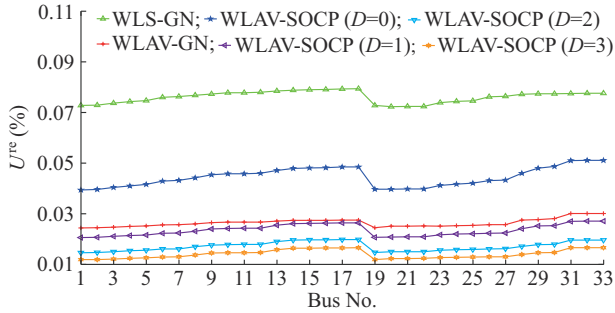| Method	U^{re} (%)	θ^{ae} (°)	E^{re} (%)	E^{ae} (kW)	T^{tot} (s)
WLS-GN	0.0761	0.0185	3.7151	0.7167	7.276
WLAV-GN	0.0264	0.0036	4.3458	0.8069	10.781
WLAV-SOCP ($D=0$)	0.0445	0.0023	3.0662	0.6711	15.689
WLAV-SOCP ($D=1$)	0.0235	0.0021	2.8532	0.6352	28.526
WLAV-SOCP ($D=2$)	0.0171	0.0020	2.7498	0.6223	35.066
WLAV-SOCP ($D=3$)	0.0140	0.0020	2.6853	0.6096	44.029

Fig. 7. Estimation errors of nodal voltage magnitudes with different methods.

The results show that when the coefficient D is 0, the estimation errors of nodal voltage phase angles and nodal power injections outperform the other two methods. When the coefficient D increases to 1, the estimation errors of nodal voltage magnitudes are also superior to other methods. With the increase of coefficient D, the estimation errors of nodal power injections show a certain reduction.

C. Robustness to Bad Data Analysis

The bad measurement data are simulated by adding relatively large Gaussian distributed errors to the corresponding true values. The relatively large measurement error is usually set to be larger than 5 times the normal measurement standard deviation. The estimation results of the WLAV-SOCP method are intended to illustrate the robustness to bad measurement data.

1) Single Bad Measurement Data

Single bad measurement data is set in each state estimation, and all the bad measurement data are distributed at different nodes or lines. The multi-source measurement configurations are still based on Fig. 6. A total of 250 Monto Carol simulations are performed. No extra post-estimation bad data identification is processed in all three methods.

The results in Table IX indicate that without the post-estimation bad data processing, the estimation accuracy of the WLS-GN method is evidently larger than that of the WLAV-based estimators. In contrast, the WLAV-based estimators including the WLAV-GN method and the WLAV-SOCP method exhibit the property of automatic bad data rejection.

TABLE IX
COMPARISON OF STATE ESTIMATION RESULTS WITH SINGLE BAD MEASUREMENT DATA

Method	U^{re} (%)	θ^{ae} (°)	E^{re} (%)	E^{ae} (kW)	T^{tot} (s)
WLS-GN	0.1819	0.0367	7.3114	1.4029	7.983
WLAV-GN	0.0284	0.0036	6.4462	1.1113	11.208
WLAV-SOCP ($D=0$)	0.0467	0.0030	4.2436	0.8702	16.725
WLAV-SOCP ($D=1$)	0.0240	0.0024	3.0135	0.6759	30.080
WLAV-SOCP ($D=2$)	0.0175	0.0023	2.9268	0.6640	36.001
WLAV-SOCP ($D=3$)	0.0143	0.0023	2.8468	0.6474	44.488

With the utilization of multi-time slots of D-PMU measurements, the proposed WLAV-SOCP method can identify and correct the bad measurement resulting from the failure of network communication or sudden abnormal measurement. By comparing the results in Table VIII and Table IX, the estimation accuracy considering the single bad measurement data is close to the scenario where there is no bad measurement. It can be extended to the bad measurement scenario where more than one non-conforming bad data measurement, which is not described here.

2) Multiple Conforming Bad Measurement Data

To describe the effectiveness of the proposed method, the measurement scenarios including multiple conforming bad measurement data are described as follows.

Case 1: the sending-end current magnitude measurement value of D-PMUs in the line connecting nodes 5 and 6 (D-I-5-6) increases from 121.6582 A to 133.6582 A, and the receiving-end active power measurement value in the line connecting nodes 6 and 7 (P-6-7) decreases from −364.4283 kW to −437.6068 kW.

Case 2: the sending-end current magnitude measurement value of D-PMUs in the line connecting nodes 1 and 2 (D-I-1-2) increases from 197.2925 A to 237.0729 A, and the sending-end active power measurement value in the line connecting nodes 1 and 2 (P-1-2) increases from 1219.3742 kW to 1445.9194 kW.

Case 3: the sending-end current magnitude measurement value of D-PMUs in the line connecting nodes 2 and 3 (D-I-2-3) decreases from 179.4144 A to 161.2107 A, and the sending-end current magnitude measurement value of D-

PMUs in the line connecting nodes 2 and 19 (D-I-2-19) increases from 18.0837 A to 36.1718 A, and the sending-end active power measurement value in the line connecting nodes 3-23 (P-3-23) decreases from 313.1989 kW to 205.8947 kW.

The coefficient of multi-time slots of D-PMU measurements D in the WLAV-SOCP method is set to be 1. The comparison of bad data identification results is shown in Table X.

TABLE X
COMPARISON OF STATE ESTIMATION RESULTS WITH MULTIPLE CONFORMING BAD MEASUREMENT DATA

	Value	Case 1		Case 2		Case 3		
		D-I-5-6 (A)	P-6-7 (kW)	D-I-1-2 (A)	P-1-2 (kW)	D-I-2-3 (A)	D-I-2-19 (A)	P-3-23 (kW)
	Measurement	121.7011, 133.6582, 121.6516	−437.6068	197.6049, 197.0091, 237.0729	1445.9194	179.3481, 161.2107, 179.3418	18.0776, 36.1718, 18.0744	205.8947
	True	121.6582	−364.4283	197.2925	1219.3742	179.4144	18.0837	313.1989
Estimation	WLS-GN	126.1285	−382.4433	221.8963	1404.0266	161.9103	36.0962	207.8455
	WLAV-GN	121.6582	−364.6023	200.7107	1242.6048	161.8424	36.1718	199.2292
	Proposed WLAV-SOCP	121.6348	−364.2590	197.2085	1219.3627	179.2867	18.0782	312.2099

It can be observed from the results in Case 1, the WLAV-GN method and the proposed WLAV-SOCP method can identify the conforming bad measurement data. However, in Case 2 and Case 3, the WLAV-GN method cannot identify the conforming bad measurement data. With the multiple time slots of D-PMU measurements, the WLAV-SOCP method identifies the sudden conforming bad measurement data in all three cases. Therefore, the robustness to multiple conforming bad measurement data of the proposed method is verified.

D. Estimation Performance in Larger-scale Distribution Networks

To verify the effectiveness of the proposed method in larger-scale distribution networks, the modified IEEE 123-node system is adopted. The topology of the modified IEEE 123-node system is presented in Fig. 8.
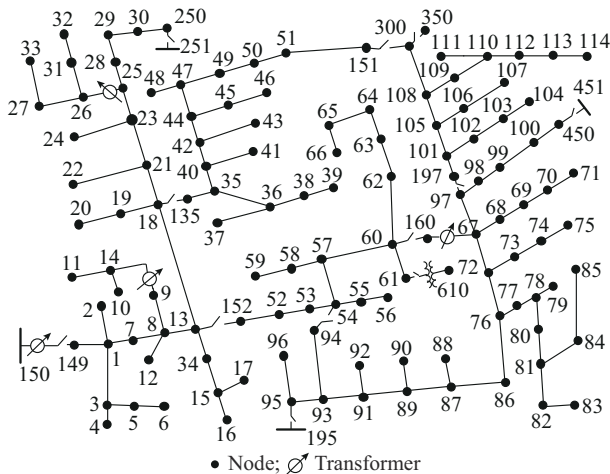

Fig. 8.   Topology of modified IEEE 123-node system.

The mutual impedances between phases are ignored and the measurement redundancy is 1.651. To assess the estimation accuracy and bad data identification of the proposed method, 100 Monte Carlo simulations are performed. The multi-source measurement scenario considering D-PMU measurements in Fig. 8 is analyzed, and the state estimation results of different methods without bad measurement data are shown in Table XI.

TABLE XI
COMPARISON OF STATE ESTIMATION RESULTS WITHOUT BAD
MEASUREMENT DATA FOR MODIFIED IEEE 123-NODE SYSTEM

Method	U^{re} (%)	θ^{ae} (°)	E^{re} (%)	E^{ae} (kW)	T^{tot} (s)
WLS-GN	0.0133	0.0015	0.3876	0.0926	23.439
WLAV-GN	0.0158	0.0019	0.3063	0.0738	27.327
WLAV-SOCP ($D=0$)	0.0255	0.0026	0.6218	0.1556	43.345
WLAV-SOCP ($D=1$)	0.0155	0.0015	0.3765	0.0963	69.403
WLAV-SOCP ($D=2$)	0.0099	0.0009	0.3335	0.0861	87.773
WLAV-SOCP ($D=3$)	0.0076	0.0008	0.3154	0.0817	110.373

Note: total computation time T^{tot} refers to total time of 100 simulations.

The state estimation results in Table XI indicate that when the coefficient of multi-time slots of D-PMUs D is 1, the estimation errors of nodal voltage magnitudes reduce to 0.0155%, which is competitive with the other two methods. In addition, with the increase of coefficient D, the estimation errors in nodal power injections show a certain reduction.

Similar to the bad measurement data scenarios in Section IV-C, to illustrate the robustness to bad measurement data of the proposed method, three bad measurement data are set in each state estimation and all the bad measurement data are distributed at different nodes or lines. The state estimation results of different methods with three bad measurement data are shown in Table XII.

The above estimation results indicate that with the utilization of multiple time slots of D-PMU measurements, the proposed WLAV-SOCP method can identify the bad measurement data in the multi-source measurements. Although the proposed method takes a relatively long computation time, the computation time of single state estimation is still less than 1 s, which is within the acceptable range.

TABLE XII
COMPARISON OF STATE ESTIMATION RESULTS WITH THREE BAD
MEASUREMENT DATA FOR MODIFIED IEEE 123-NODE SYSTEM

Method	U^{re} (%)	θ^{ae} (°)	E^{re} (%)	E^{ae} (kW)	T^{tot} (s)
WLS-GN	0.0155	0.0028	0.9268	0.2243	**25.832**
WLAV-GN	0.0160	0.0019	0.5009	0.1227	27.986
WLAV-SOCP ($D=0$)	0.0264	0.0026	0.7991	0.2000	45.544
WLAV-SOCP ($D=1$)	0.0155	0.0015	0.3783	0.0966	73.020
WLAV-SOCP ($D=2$)	0.0099	0.0009	0.3334	0.0859	87.530
WLAV-SOCP ($D=3$)	0.0075	0.0007	0.3158	0.0818	109.238

Note: bolded number means that there exists 3 times non-convergence in
WLS-GN method.

V. CONCLUSION

An SOCP-based RSE method considering the multi-source measurements in ADNs is proposed in this paper. The method incorporates measurement data consisting of D-PMUs, SCADA, and AMI. A linearized estimation model of multi-source measurements related to the SOCP state variables is formulated. The phase angle measurements of D-PMUs are converted to the equivalent power measurements. The revised SOCP-based WLAV method transforms the non-convex problem into the convex problem and is carried out to improve the estimation accuracy and convergence of state estimation. Estimation results in the modified IEEE 33-node and IEEE 123-node systems indicate that with the multiple time slots of D-PMU measurements, the trade-off between the estimation accuracy and computational efficiency of the proposed method is realized. The robustness to the single bad measurement data and the multiple conforming bad measurement data of the proposed method is verified.

REFERENCES

[1] I. Kouveliotis-Lysikatos, N. Hatziargyriou, Y. Liu *et al.*, "Towards an Internet-like power grid," *Journal of Modern Power Systems and Clean Energy*, vol. 10, no. 1, pp. 1-11, Jan. 2022.

[2] M. L. Hossain, A. Abu-Siada, S. M. Muyeen *et al.*, "Industrial IoT based condition monitoring for wind energy conversion system," *CSEE Journal of Power and Energy Systems*, vol. 7, no. 3, pp. 654-664, May 2021.

[3] A. G. Phadke and J. S. Thorp, *Synchronized Phasor Measurements and Their Applications*. New York: Springer, 2008.

[4] H. Su, C. Wang, P. Li *et al.*, "Novel voltage-to-power sensitivity estimation for phasor measurement unit-unobservable distribution networks based on network equivalent," *Applied Energy*, vol. 250, pp. 302-312, Sept. 2019.

[5] C. Feng, Y. Wang, Q. Chen *et al.*, "Smart grid encounters edge computing: opportunities and applications," *Advances in Applied Energy*, vol. 1, p. 100006, Feb. 2021.

[6] M. Naguib, W. A. Omran, and H. E. A. Talaat, "Performance enhancement of distribution systems via distribution network reconfiguration and distributed generator allocation considering uncertain environment," *Journal of Modern Power Systems and Clean Energy*, vol. 10, no. 3, pp. 647-655, May 2022.

[7] M. Huang, Z. Wei, J. Zhao *et al.*, "Robust ensemble Kalman filter for medium-voltage distribution system state estimation," *IEEE Transactions on Instrumentation and Measurement*, vol. 69, no. 7, pp. 4114-4124, Jul. 2020.

[8] R. A. Jabr, "Power flow based volt/var optimization under uncertainty," *Journal of Modern Power Systems and Clean Energy*, vol. 9, no. 5, pp. 1000-1006, Sept. 2021.

[9] Y. Huo, P. Li, H. Ji *et al.*, "Data-driven adaptive operation of soft open points in active distribution networks," *IEEE Transactions on Industrial Informatics*, vol. 17, no. 12, pp. 8230-8242, Dec. 2021.

[10] A. Primadianto and C. Lu, "A review on distribution system state estimation," *IEEE Transactions on Power Systems*, vol. 32, no. 5, pp. 3875-3883, Sept. 2017.

[11] H. Su, C. Wang, P. Li *et al.*, "Optimal placement of phasor measurement unit in distribution networks considering the changes in topology," *Applied Energy*, vol. 250, pp. 313-322, Sept. 2019.

[12] A. Al-Wakeel, J. Wu, and N. Jenkins, "State estimation of medium voltage distribution networks using smart meter measurements," *Applied Energy*, vol. 184, pp. 207-218, Dec. 2016.

[13] H. Dharmawardena and G. K. Venayagamoorthy, "A distributed data-driven modelling framework for power flow estimation in power distribution systems," *IET Energy System Integration*, vol. 3, no. 3, pp. 367-379, Sept. 2021.

[14] M. Göl and A. Abur, "A hybrid state estimator for systems with limited number of PMUs," *IEEE Transactions on Power Systems*, vol. 30, no. 3, pp. 1511-1517, May 2015.

[15] T. Wu, C. Y. Chung, and I. Kamwa, "A fast state estimator for systems including limited number of PMUs," *IEEE Transactions on Power Systems*, vol. 32, no. 6, pp. 4329-4339, Nov. 2017.

[16] I. Džafić, R. A. Jabr, I. Huseinagić *et al.*, "Multi-phase state estimation featuring industrial-grade distribution network models," *IEEE Transactions on Smart Grid*, vol. 8, no. 2, pp. 609-618, Mar. 2017.

[17] Y. Ju, W. Wu, F. Ge *et al.*, "Fast decoupled state estimation for distribution networks considering branch ampere measurements," *IEEE Transactions on Smart Grid*, vol. 9, no. 6, pp. 6338-6347, Nov. 2018.

[18] I. Džafić, R. A. Jabr, and T. Hrnjić, "Complex variable multi-phase distribution system state estimation using vectorized code," *Journal of Modern Power Systems and Clean Energy*, vol. 8, no. 4, pp. 679-688, Jul. 2020.

[19] Q. Li, L. Cheng, W. Gao *et al.*, "Fully distributed state estimation for power system with information propagation algorithm," *Journal of Modern Power Systems and Clean Energy*, vol. 8, no. 4, pp. 627-635, Jul. 2020.

[20] P. M. De Oliveira-De Jesus, N. A. Rodriguez, D. F. Celeita *et al.*, "PMU-based system state estimation for multigrounded distribution systems," *IEEE Transactions on Power Systems*, vol. 36, no. 2, pp. 1071-1081, Mar. 2021.

[21] D. P. Bertsekas, *Nonlinear Programming*, 2nd ed. Belmont: Athena Scientific, 1999.

[22] California ISO, "Five year synchrophasor plan," California ISO, Folsom, USA, Nov. 2011.

[23] J. Zhao and L. Mili, "Sparse state recovery versus generalized maximum-likelihood estimator of a power system," *IEEE Transactions on Power Systems*, vol. 33, no. 1, pp. 1104-1106, Jan. 2018.

[24] Y. Chen, J. Ma, P. Zhang *et al.*, "Robust state estimator based on maximum exponential absolute value," *IEEE Transactions on Smart Grid*, vol. 8, no. 4, pp. 1537-1544, Jul. 2017.

[25] H. Singh and F. L. Alvarado, "Weighted least absolute value state estimation using interior point methods," *IEEE Transactions on Power Systems*, vol. 9, no. 3, pp. 1478-1484, Aug. 1994.

[26] M. Göl and A. Abur, "LAV based robust state estimation for systems measured by PMUs," *IEEE Transactions on Smart Grid*, vol. 5, no. 4, pp. 1808-1814, Jul. 2014.

[27] R. A. Jabr and B. C. Pal, "Iteratively reweighted least-squares implementation of the WLAV state-estimation method," *IEE Proceedings: Generation, Transmission and Distribution*, vol. 151, no. 1, pp. 103-108, Jan. 2004.

[28] M. Dorier, G. Frigo, A. Abur *et al.*, "Leverage point identification method for LAV-based state estimation," *IEEE Transactions on Instrumentation and Measurement*, vol. 70, p. 1008810, Jul. 2021.

[29] Y. Chen, F. Liu, S. Mei *et al.*, "A robust WLAV state estimation using optimal transformations," *IEEE Transactions on Power Systems*, vol. 30, no. 4, pp. 2190-2191, Jul. 2015.

[30] Y. Lin and A. Abur, "Robust state estimation against measurement and network parameter errors," *IEEE Transactions on Power Systems*, vol. 33, no. 5, pp. 4751-4759, Sept. 2018.

[31] M. Farivar and S. H. Low, "Branch flow model: relaxations and convexification – part I," *IEEE Transactions on Power Systems*, vol. 28, no. 3, pp. 2554-2564, Aug. 2013.

[32] S. H. Low, "Convex relaxation of optimal power flow–part I: formulations and equivalence," *IEEE Transactions on Control of Network Systems*, vol. 1, no. 1, pp. 15-27, Mar. 2014.

[33] R. Madani, J. Lavaei, and R. Baldick, "Convexification of power flow equations in the presence of noisy measurements," *IEEE Transactions on Automatic Control*, vol. 64, no. 8, pp. 3101-3116, Aug. 2019.

[34] Y. Yao, X. Liu, D. Zhao *et al.*, "Distribution system state estimation: A semidefinite programming approach," *IEEE Transactions on Smart*

Grid, vol. 10, no. 4, pp. 4369-4378, Jul. 2019.

[35] Y. Zhang, R. Madani, and J. Lavaei, "Conic relaxations for power system state estimation with line measurements," *IEEE Transactions on Control of Network Systems*, vol. 5, no. 3, pp. 1193-1205, Sept. 2018.

[36] G. Wang, H. Zhu, G. B. Giannakis *et al.*, "Robust power system state estimation from rank-one measurements," *IEEE Transactions on Control of Network Systems*, vol. 6, no. 4, pp. 1391-1403, Dec. 2019.

[37] H. Ji, C. Wang, P. Li *et al.*, "An enhanced SOCP-based method for feeder load balancing using the multi-terminal soft open point in active distribution networks," *Applied Energy*, vol. 208, pp. 986-995, Dec. 2017.

[38] P. Li, J. Ji, H. Ji *et al.*, "Self-healing oriented supply restoration method based on the coordination of multiple SOPs in active distribution networks," *Energy*, vol. 195, p. 116968, Mar. 2020.

[39] Y. Chen, Y. Yao, and Y. Zhang, "A robust state estimation method based on SOCP for integrated electricity-heat system," *IEEE Transactions on Smart Grid*, vol. 12, no. 1, pp. 810-820, Jan. 2021.

[40] J. R. Taylor, *An Introduction to Error Analysis, The Study of Uncertainties in Physical Measurements.* Sausalito, USA: University Science Books, 1997.

[41] E. D. Andersen, C. Roos, and T. Terlaky, "On implementing a primal-dual interior-point method for conic quadratic optimization," *Mathematical Programming*, vol. 95, no. 2, pp. 249-277, Feb. 2003.

[42] MOSEK Fusion API for C++. （2022，Apr.）. MOSEK ApS, Copenhagen, Denmark. [Online]. Available: https://docs.mosek.com/latest/cxxfusion/index.html

Zhelin Liu received the B. S. and M. S. degrees in electrical engineering from Tianjin University, Tianjin, China, in 2013 and 2016, respectively. He is currently pursuing the Ph. D. degree in electrical engineering in Tianjin University. His current research interest includes distribution network state estimation.

Peng Li received the B.S. and Ph.D. degrees in electrical engineering from Tianjin University, Tianjin, China, in 2004 and 2010, respectively. He is currently a Professor with the School of Electrical and Information Engineering, Tianjin University. His current research interests include operation and planning of active distribution networks, modelling and transient simulation of power systems.

Chengshan Wang received the Ph.D. degree in electrical engineering from Tianjin University, Tianjin, China, in 1991. He is currently a Professor with the School of Electrical and Information Engineering, Tianjin University. Prof. Wang is a Member of the Chinese Academy of Engineering. His research interests include distribution system analysis and planning, distributed generation, and microgrids.

Hao Yu received the B.S. and Ph.D. degrees in electrical engineering from Tianjin University, Tianjin, China, in 2010 and 2015, respectively. He is currently an Associate Professor with the School of Electrical and Information Engineering, Tianjin University. His current research interests include operation analysis and optimization of active distribution networks and integrated energy systems.

Haoran Ji received the B. S. and Ph. D. degrees in electrical engineering from Tianjin University, Tianjin, China, in 2014 and 2019, respectively. From 2019 to 2021, he was a Postdoctoral Researcher with Tianjin University. He is currently an Associate Professor with the School of Electrical and Information Engineering, Tianjin University. His research interests include distributed generation and optimal operation of distribution networks.

Wei Xi received the M.S. degree from Huazhong University of Science and Technology, Wuhan, China, in 2003. He is currently a Senior Engineer with the Digital Grid Research Institute, China Southern Power Grid, Guangzhou, China. He is pursuing the Ph. D. degree in electrical engineering in Tianjin University, Tianjin, China. His current research interests include electric power chip development and digitization of power grid.

Jianzhong Wu received the B.S., M.S., and Ph.D. degrees in electrical engineering from Tianjin University, Tianjin, China, in 1999, 2002, and 2004, respectively. He is currently a Professor of multi-vector energy systems and the Head of School of Engineering, Cardiff University, Cardiff, U. K. His current research interests include integrated multi-energy infrastructure and smart grids.